Energy 89 (2015) 678–686

Contents lists available at ScienceDirect

Energy

journal homepage: www.elsevier.com/locate/energy

# Performance analysis and SOH (state of health) evaluation of lithium polymer batteries through electrochemical impedance spectroscopy

Matteo Galeotti [a, *], Lucio Cinà [a, c], Corrado Giammanco [a, c], Stefano Cordiner [b, c], Aldo Di Carlo [a, c]

[a] Department of Electronic Engineering, University of Rome Tor Vergata, Via del Politecnico 1, 00133 Rome, Italy
[b] Department of Industrial Engineering, University of Rome Tor Vergata, Via del Politecnico 1, 00133 Rome, Italy
[c] CHOSE (Center for Hybrid and Organic Solar Energy), Via Giacomo Peroni 400/402, 00131 Rome, Italy

ARTICLE INFO

*Article history:*
Received 10 January 2015
Received in revised form
4 May 2015
Accepted 30 May 2015
Available online 2 July 2015

*Keywords:*
Batteries
State of charge
State of health
Lithium polymer
Electrochemical impedance spectroscopy

ABSTRACT

Electrochemical energy storage has become important in the last years to improve the energetic efficiency of stationary and hybrid energy production systems. Lithium batteries represent the best choice, since they have high energy and power density, high number of cycles and a good temperature behaviour compared to other technologies. It becomes important the monitoring of the state of the battery to know online the energy content, to avoid dangerous operating conditions and to extend the useful life. In this work, we have defined a test procedure to study the ageing of LiPO (lithium polymer) batteries through the EIS (electrochemical impedance spectroscopy) technique. Through a fitting procedure performed on the acquired IS (impedance spectra), we have extracted the parameters of an equivalent circuit model to reproduce the voltage discharge curves of the batteries and to study the performance under load. Then we have introduced a relation between the ohmic resistance of the battery and the available capacity to evaluate the SOH (state of health) through the ToE (Theory of Evidence). The method is able to detect the SOH of the tested batteries with a maximum error of 3.73%, with an enhancement to 8.66% when an anomalous cell is considered.



## 1. Introduction

Lithium batteries have experienced a growing interest in automotive, stationary and hybrid energy production systems [1–5]. High energy density, power density and number of cycles are the principal reasons for their exploitation. In these systems, for example in EV (electric vehicles), the use of lithium electrochemical cells requires however special care in the evaluation of the state of the batteries [6,7], particularly the SOH [8,9], an indication of the battery failure. The SOH is however a difficult parameter to determine. Indeed, since lithium batteries are electrochemical devices, they are subjected to continuous degradation during operation and storage [10]. In some applications, for example in EV and PHEV (plug-in hybrid electric vehicles), high and variable rate cycling and fast transitions from discharge to charge accelerates the ageing processes [11]. The ageing mechanism is also correlated to the particular materials constituting the cell and to its manufacturing process [12]. However in general the degradation occurs at the interface between the electrolyte and the electrodes and it is due to the growth of the SEI (Solid Electrolyte Interface) film on the anode side of the battery [13]. The degradation of the cell leads to the capacity fade, due to the active lithium consumption, and power fade, caused by the impedance growth due to an increase of the SEI thickness [14]. These two phenomena occur at the same time during the degradation of the cell, but the complex relationship between them [15] requires an individual identification. Most of the on-line SOH estimation solutions in the literature follow the scheme systematically applied in Refs. [16,17] which is based on a phenomenological modelling of the cell and consists of SOC (state of charge) estimation through a KF (Kalman Filter) and a parallel identification of the model lumped parameters. In Ref. [18] this approach is validated with experimental tests using stepwise current profiles and the only resistance growth as an indicator of the SOH. A recursive least squares minimization criterion is used by Xiao-song et al. [19] and Hu et al. [20] for the identification of all parameters of the equivalent circuital model for a fresh cell. The methods based on KF are particularly useful in the SOC estimation,

* Corresponding author. Tel.: +39 0672597783; fax: +39 0672597939.
*E-mail address:* matteo.galeotti@uniroma2.it (M. Galeotti).

http://dx.doi.org/10.1016/j.energy.2015.05.148
0360-5442/

but the necessity to determine the correct initial guess combined with a parallel estimation of the model parameters makes the KF not particularly adapted for the SOH estimation. Recently several methods, based on the EIS (electrochemical impedance spectroscopy) technique [21], have been used for the estimation of the SOH. EIS is a good diagnostic method to study the physical and chemical effects that occur inside an electrochemical system to evaluate its state [22–24]. In the SOH problems, EIS is mainly used to determine the impedance spectrum of the battery with a following analysis of an equivalent model parameters, extracted through a fitting procedure of the experimental IS (impedance spectra). The variation of the parameters is then used to study the ageing mechanisms of the battery [25–29]. However rarely the parameters are used to study the performance of the battery under discharge load condition and online, when the battery is operative. In this paper we have characterized LiPO batteries of 3.7 V and 1.05 Ah of nominal voltage and capacity respectively through the EIS technique. We have defined a protocol test to study the ageing effects of the LiPO cells and we have acquired the IS at different SOC and SOH. We have extracted the physical parameters of the batteries through an equivalent circuit model, making a fitting procedure on the IS. The variation of the parameters with the SOC and the SOH is then used to study the performance online of the batteries, useful when they are integrated in stationary and hybrid energy production systems. In the end we have introduced a relation between the ohmic resistance and the available capacity of the battery to quickly determine the SOH through the formalism of the Dempster-Schafer ToE. In section 2 is reported the equivalent circuit model used to reproduce the IS. The experimental setup and the test procedure used to age the cells are described in section 3. In section 4.1 the parameters of an equivalent circuit model are extracted from the experimental IS and are used in section 4.2 to reproduce the voltage discharge curves of the batteries, evaluating the performance of the cells. In section 4.3 a diagnostic map, based on the variation of the ohmic resistance of the battery, is defined to determine the SOH through the ToE.

## 2. Modelling of the impedance data

The physical effects that occur in any electrochemical system can be associated to the electrical parameters of a circuit model, useful to quantify the phenomena that occur inside the battery during charging, discharging and ageing processes. The equivalent circuit can therefore represents the IS. To model the battery, we use an extension of the Randles circuit model [33] and it is reported in Fig. 1. The proposed equivalent circuit is general and can be used to reproduce the impedance spectra of a battery (each technology and capacity values). Indeed, the impedance spectra of a cell are usually reproduced using a resistance (ohmic effect), two parallel ZARC elements (reproduction of the two semicircles in the Nyquist plane, related to the electrodes of the cell) and a diffusion element (in this case a constant phase element) to reproduce the Warburg diffusion phenomena. Farther the proposed model can reproduce the impedance spectra of a battery at different state of charge and different state of health (as demonstrated in section 4). The only limit regards the choice of the initial values of the model parameters: more they are distant from the true value, more the model could have difficulties to reach the convergence and extract the parameters. This can be a problem if the batteries suddenly experience important failure conditions (short circuits, overvoltage, etc), resulting an immediate rupture that can sharp change the electrical parameters. The advantages of the proposed model can be therefore summarized in the next points:

- two time constants (parallel $CPE//R_{ct}$) are used to separate the electrodes effects (anode and cathode processes).
- constant phase elements are used (instead of ideal capacitors) to reproduce non ideality of the electrodes surfaces (roughness of the electrodes).
- a Warburg element is used to reproduce diffusion phenomena when the applied frequencies are low (order of mHz).

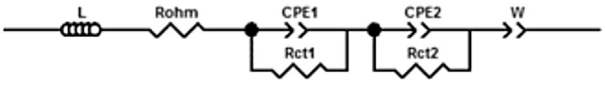


**Fig. 1.** Battery equivalent circuit.

The electrical elements of the circuit are correlated to the different phenomena that occur inside the battery. For example, $L$ reproduces the inductive behaviour, principally due to the connections between the device and the elements of the system. $R_{ohm}$ represents the effects of the ohmic resistance of the electrodes and electrolyte of the battery. The two parallel elements $CPE//R_{ct}$ are used to represent the processes that occur at the interface electrodes/electrolyte. The $CPE$ (constant phase element) represents the formation of double layer capacity, while $R_{ct}$ is the charge transfer resistance at the electrodes. The element $W$ is the Warburg impedance, used to reproduce the diffusion phenomena of the ions in the electrolyte during the discharging and charging processes. The impedance expression of the elements of the circuit can be expressed as:

$$Z_L = j\omega L \tag{1}$$

$$Z_R = R_\Omega \tag{2}$$

$$Z_{ARC1} = \frac{R_{ct1}}{1 + R_{ct1}C_{PE1}(j\omega)^{n_1}} \tag{3}$$

$$Z_{ARC2} = \frac{R_{ct2}}{1 + R_{ct2}C_{PE2}(j\omega)^{n_2}} \tag{4}$$

$$Z_{CPEW} = \frac{1}{C_{PEW}(j\omega)^{n_W}} \tag{5}$$

The total impedance of the battery assumes the following form:

$$Z_{TOT} = Z_L + Z_R + Z_{ARC1} + Z_{ARC2} + Z_{CPEW} \tag{6}$$

$Z_L$ is the impedance of the inductor. $R_\Omega$ is the ohmic resistance. $Z_{ARC1}$ and $Z_{ARC2}$ are respectively the impedance values of the $C_{PE1}//R_{ct1}$ and $C_{PE2}//R_{ct2}$ elements of the circuit [34]. The $n$ at the denominator of the expressions denotes an angle that rotates in the complex plane relative to a pure capacity behaviour. If $n = 1$, the impedance is a pure capacitor, if $n = 0$, the result is a pure resistance. $Z_{CPEW}$ is the impedance of the constant phase element used to reproduce the diffusion phenomena. With a non linear fitting procedure performed on the experimental IS, it is possible to obtain the parameters of the equivalent circuit model, necessary to reconstruct the discharge curves of the cells, to study their cycling performance and to understand if they are having an anomalous ageing during operation. Besides, some parameters vary with the ageing of the battery and can be used to determine the SOH.

## 3. Experimental

Several test procedures exist in the literature to accelerate the ageing mechanisms of the lithium batteries. Some authors use a protocol test where the lithium batteries are cycled at high

temperature to study the capacity fade [30]. Other works use high discharge rates to determine the loss of capacity during cycling [31]. Our test procedure consists of repeated discharges and recharges of the cell at high C-rate. Every 45 cycles, we have performed a standard discharge to determine the loss of capacity. During these standard discharges, we have acquired the IS at different SOC to study the ageing mechanisms through the EIS. The procedure is reported in Fig. 2. We have realized an experimental setup composed by a Keithley 2420 Source Meter for the discharging and charging processes of the batteries, a Gamry Instruments Series G 300 potentiostat to collect IS and an opto-isolated relay board (Devantech RLY816) to enable the connections between battery, Keithley and Gamry. We have controlled all the elements of the experimental setup through LabVIEW. The elements of the experimental setup are reported in Fig. 3. In the inset of Fig. 3 the connections between the elements are shown. In the test procedure, the recharge of the battery is composed by two steps: a constant current recharge at 1C-rate (1 A) until a maximum voltage of 4.2 V, followed by a constant voltage recharge until a detection of a minimum current of 0.2 A. The discharge is performed in constant current mode at 1C-rate until the voltage of the cell reaches a cut-off of 2.75 V. We utilize the standard discharge at the begin of the algorithm to determine the available capacity of the battery. The acquisition of the IS occurs in galvanostatic mode, to better control the working point of the battery and to limit the errors during the acquisition of the data. The temperature is kept constant at 25 °C thanks to a Peltier based temperature control. The current signal amplitude has been set to 40 mA rms that corresponds to a variation on the output voltage of the cell of a value smaller than 10 mV (in this condition we can consider the system linear). The applied frequencies sweep from 5 kHz to 0.2 Hz (45 applied frequencies). We have acquired the IS at different SOC after a partial discharge of 360 s in constant current mode at 1C-rate. We have waited 5 min of relaxation time before the acquisition of the

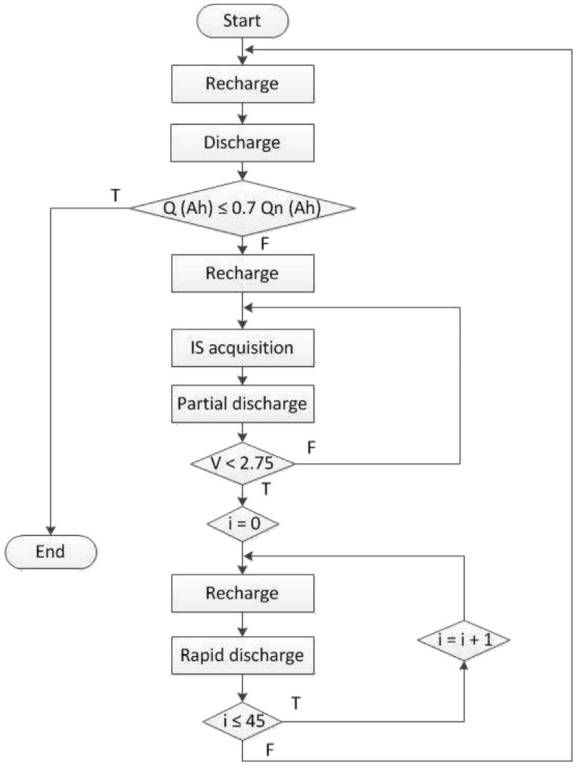


**Fig. 2.** Experimental test procedure.

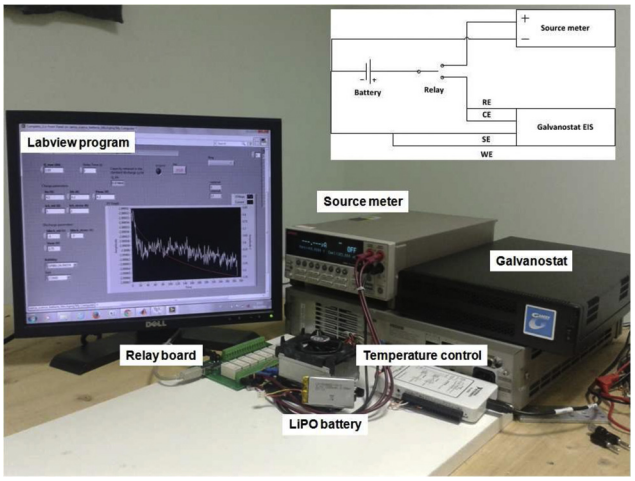


**Fig. 3.** Experimental setup.

IS, to stabilize the OCV (open circuit voltage) and the temperature of the battery. Once the voltage of the battery reaches the cut-off, the accelerated protocol test will start. This phase consists of a 45 complete charge and discharge cycles of the battery, and it is necessary to accelerate the ageing mechanisms of the cell. In this step we have performed the discharge process with a constant current equal to 3C-rate (3 A) until the voltage of the cell reaches the cut-off value. The entire algorithm is repeated until the released capacity becomes smaller than 70% of the nominal capacity.

## 4. Results and discussion

In this work we have tested four LiPO cells. Excluding the section 4.3, where a diagnostic map is built to compare the tested cells and to determine the SOH through the ToE, we report only the results of a reference battery. In Fig. 4a are reported the discharge curves of the reference battery during the ageing. The battery experiences a voltage decrease with a resulting reduction of the available capacity. In Fig. 4b is reported the trend of the available charge (the

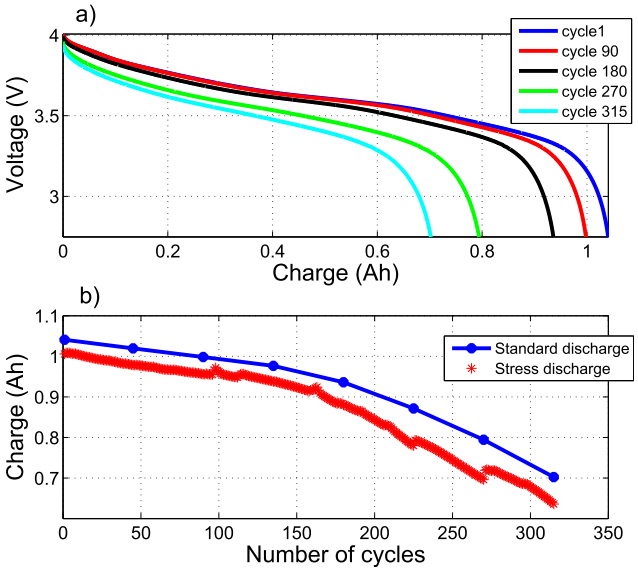


**Fig. 4.** a) Voltage discharge curves of the battery. b) Trend of the capacity versus number of cycles of the battery during the standard and stress discharge condition.

available capacity of the cell) during the standard and stress protocol test. It is possible to see that the capacity versus number of cycles shows an initial linear behaviour, followed by a steep reduction after 160 cycles. This trend is the same for all the lithium technology [32]. The trend of the capacity during the stress test has the same behaviour but smaller values compared to the standard procedure. This is due to a bigger current discharge that results in a loss of energetic efficiency, due to a bigger voltage drop at the begin of the discharge.

### 4.1. Impedance analysis

Figs. 5 and 6 show the comparison between experimental IS and the equivalent circuit model (Fig. 1) results at different SOC and SOH. The IS are reported in a Nyquist diagram that shows the imaginary part of the impedance versus the real part of the impedance of the battery. The Nyquist diagram shows the different physical phenomena that occur inside the battery during the charging and discharging processes. The positive imaginary impedance corresponds at the inductive phenomena, related to the cell interconnections. The negative imaginary impedance corresponds to the capacitive phenomena that establish at the interface between electrodes and electrolyte, the formation of the double layer capacitances and the effects of the charge transfer resistances. The intersection between the spectra and the real axis indicates the ohmic resistance, due to the electrodes and electrolyte resistance. The straight line at low frequency is related to the diffusion phenomena of the ions in the half cells. As shown in Fig. 5, at high SOC only one semicircle is noticed, but the effect of both electrodes are overlapped, because the two time constants are the same. A second semicircle can be observed at low SOC, an indication that the time constants of the electrodes are different. In this case the two electrodes are visible in the Nyquist diagram. Fig. 6 shows the typical trend of the IS of a lithium battery when it is fully charged. Except the first cycle of activation, the total module of the impedance enhances with the ageing. The parameters of the circuit with the SOC and the SOH, extracted through the non linear fitting procedure on the IS data are shown in Figs. 7 and 8. In Fig. 7 the ohmic resistance of the battery ($R_{ohm}$) is reported versus the SOC and at different number of cycles. As it is possible to notice, the ohmic resistance enhances during the ageing, but it remains mostly constant during the discharge cycle. Excluding the ageing effects related to the temperature, the enhancement of the ohmic

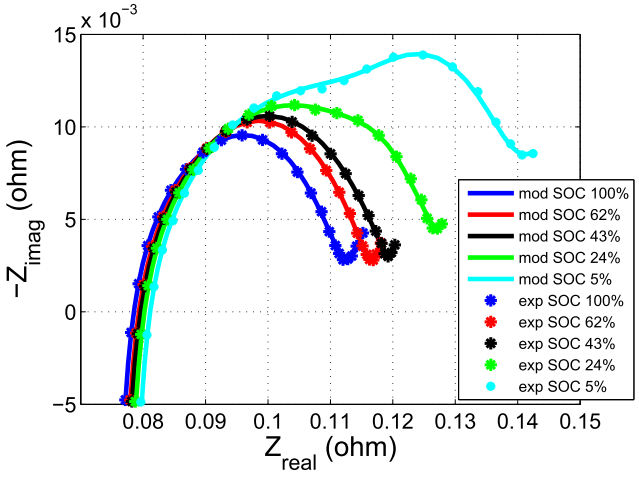


**Fig. 5.** Experimental versus model data. IS acquired at different SOC after 1 cycle of utilization (operating temperature 25 °C).

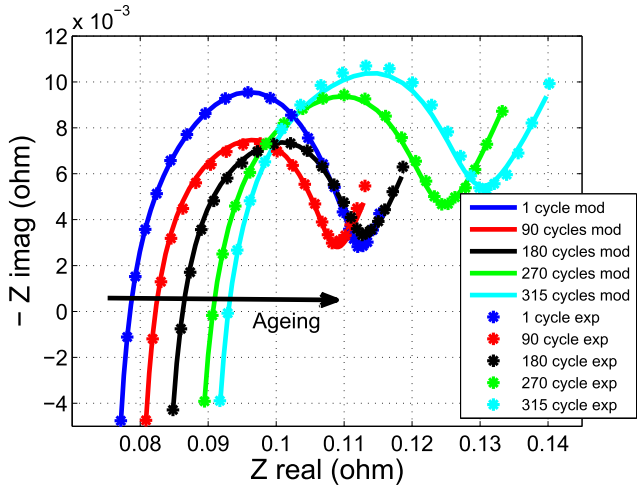


**Fig. 6.** Experimental versus model data. IS acquired at different number of cycles (operating temperature 25 ° C).

resistance with the ageing is probably due to a growth of the SEI on the anode side of the battery, and it is one of the principal reasons of the lithium battery failure [35]. The different curves are quite distant between them. This behaviour is useful to determine the SOH through the definition of a diagnostic map, that we will introduce in section 4.3. The variation of the charge transfer resistances and double layer capacitances are reported in Fig. 8. The trend of the double layer capacitances at the electrodes is an enhancement at low SOC. About the charge transfer resistances, $R_{ct1}$ enhances after the battery reaches a SOC of about 40%, while $R_{ct2}$, excluding the first cycle, remains mostly constant. In both cases, the trend of the $R_{ct}$ elements are not completely clear and it is difficult to use them to predict the SOC or the SOH. Finally, the time constants of both electrodes are shown. The *tau* elements have been obtained multiplying the charge transfer resistances and double layer capacitances of the electrodes and are related principally to the relaxation time of the battery at the begin of the discharging process [36]. In this case, the time constants includes the information of the *Rct* and *CPE* elements, and the trend is an enhancement at low SOC. It is however difficult extract useful information at different SOH. In the next paragraph, we use the EIS parameters to reproduce the discharge curve of a battery through a modified version of the equivalent circuit of Fig. 1, to study the battery performance under load.

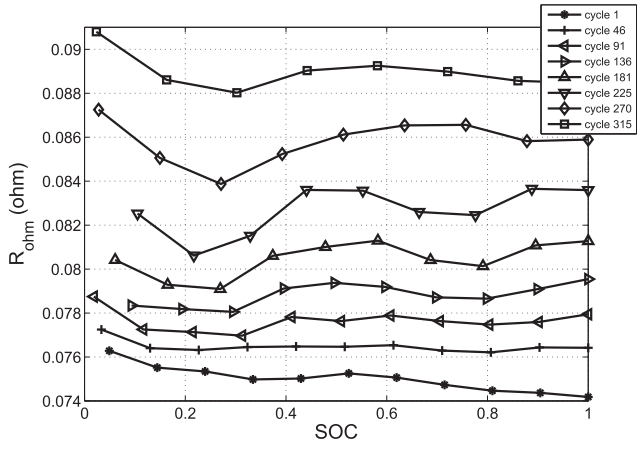


**Fig. 7.** Ohmic resistance of the battery versus SOC and at different number of cycles.

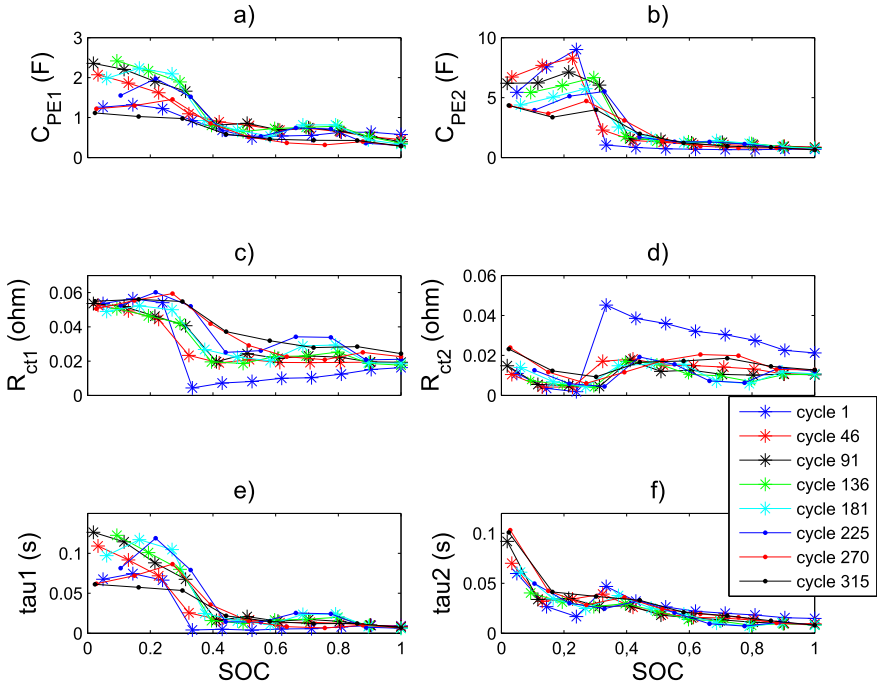


**Fig. 8.** Variation of the parameters of the equivalent circuit model versus SOC and at different number of cycles. a) $C_{PE1}$ vs SOC. b) $C_{PE2}$ vs SOC. c) $R_{ct1}$ vs SOC. d) $R_{ct2}$ vs SOC. e) *tau*1 vs SOC. f) *tau*2 vs SOC.

### 4.2. Study of the performance under load

The extracted model parameters at different SOC can be used to reproduce the transient behaviour of the cell, as discharge trends. In particular the initial transient is mainly influenced by the time constants of the electrodes, while the rest of the discharge curve is dominated by the resistive components and the capacity *C* of Fig. 9. In order to demonstrate the validity of the extracted model parameters, we reproduce the discharge curves of the battery. A good fit can be obtained from a simplified version of the equivalent circuit model of Fig. 1, where *CPE* are replaced from ideal capacitors and the inductor is neglected. It is shown in Fig. 9. *C* represents the capacity of the battery and it is an indication of the SOC. To reproduce the discharge curves of the battery at different SOH, we have substituted the parameters extracted by the EIS in this equivalent circuit. In order to simplify the implemented model in Simulink, we obtain the equivalent capacitance from the relation $C = (QR)^{1/n}/R$, where $n$ is the ideality factor, $R$ is the resistance in parallel with *CPE* elements and $Q$ is the capacitive value of *CPE*. The values of $R_{ohm}$ and $R_{ct}$ elements are the resistive parameters extracted by the EIS. During the discharge of the battery, every decrement of 0.1 Ah, the parameters at the current SOC replace the previously values, according to the variations of Figs. 7 and 8. We have represented the capacity *C* as the OCV of the battery, a non linear function of the SOC. Specifically, we have evaluated the OCV with the linear interpolation method [37], obtained as the mean between the discharge and the charge curve of the battery at 1 C-rate. In Fig. 10 is reported a comparison between the first discharge cycle of the battery and the model reproduction. The OCV of the battery, obtained with the linear interpolation method is shown in black. Using the resistive parameters of the EIS, the model reproduces the discharge curve of the battery under constant discharge load. The cut-off voltage has been set to 3.3 V, because under this value the voltage of the lithium batteries reduces drastically, resulting dangerous operating conditions [38] that can

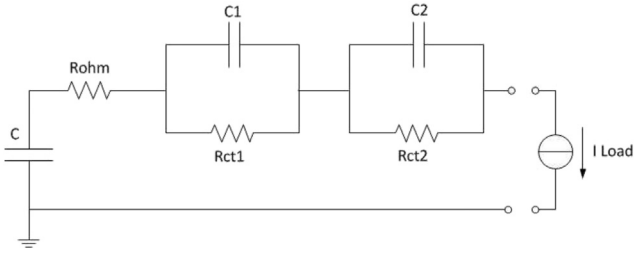


**Fig. 9.** Equivalent circuit of the battery.

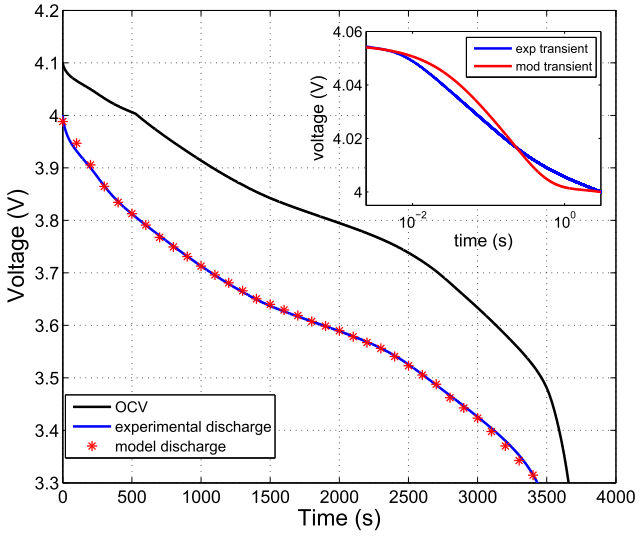


**Fig. 10.** A comparison between the first experimental discharge cycle of the battery and the model reproduction. In the inset is shown the comparison during the transient phenomena at the begin of the discharge.

shorten the remaining useful life. In the inset of Fig. 10, the model is used to reproduce the transients phenomena that occur during the initial stage of the discharge. The transient, quite well reproduced by the model, depends by the *tau* values of the electrodes, obtained by the EIS. The low error between model and experimental results is probably due to the use of ideal capacitors that substitute the constant phase elements. In Fig. 11 it is shown the comparison of the experimental data and the model reproduction of the voltage curves of the battery during the ageing. The model reproduces the experimental results with a limited error using the parameters extracted by the EIS at different SOC and SOH. As shown in Fig. 11 the model reproduces the experimental data with a maximum error of 2% along the complete discharge curve of the cell. In this section, we have reported only the data of the reference battery, but the model can reproduce the discharge curve of any tested battery of this technology. Specifically, we have tested for hundreds of cycles 4 lithium polymer batteries and the model has always reproduced the discharge curves at every cycle and at different state of health with a maximum error of 2% between the voltage experimental value and the model one, demonstrating a good reproducibility of the experimental data. The possibility to reconstruct the discharge curves of the battery is important to study the behaviour of the battery under several charge and discharge current conditions, in order to determine the SOC and the performance under load, to note if an anomalous ageing condition is occurring.

### 4.3. Estimation of the SOH through the Theory of Evidence

With the previously analysis, the discharge curves of the battery can be used to do some considerations about the SOH: for example observing the slope of the voltage discharging cycle in the linear region, it is possible to notice if an anomalous ageing is occurring. However in some applications the battery cannot be discharged completely, so it is not possible to make a correct prediction of the battery failures. This is a limit when the SOH of the battery must be evaluated online, that is the evaluation of the state of the battery while it is operative, when it is integrated in hybrid energy production systems [39,40]. In this case the batteries are subjected to a variable load and rarely they are completely discharged [41,42]. For this reason, to detect the SOH, we choose to introduce a relation between the ohmic resistance of the battery and the available capacity. We have chosen this type of diagnostic relation because the capacity fade of lithium battery is principally due to the growth of a SEI layer on anode side of the battery during cycling [43–45], that results in an increase of the internal resistance and a loss of capacity at the same time. An example of the enhancement of the ohmic resistance with the ageing is shown in Fig. 12. In this figure is reported the trend of the four LiPO batteries tested during this work. In Fig. 12a, the points of the LiPO batteries at SOC 100% are acquired at different SOH, every 45 cycles. The four curves present a different number of points, because the cycle life (number of cycles before the end of life condition) of the four batteries is different. For example the LiPO 3 had 540 cycles before it reached the cut-off of 0.7 Ah, while LiPO 2 had 315 cycles. It is possible to notice that the ohmic resistance of the four cells presents the same trend, an enhancement with the ageing (reduction of the available capacity). It is further possible to observe the same trend also at different SOC, reported in Fig. 12b and c for SOC of 70% and 40% respectively. These experimental results justify the use of a diagnostic map, built on the results acquired on the ohmic resistance, to determine the SOH. This map has been interpreted with the ToE [46]. We have already used this technique determining the cycle life of nickel-metal hydride cells [47]. In this work we use an extension of the same concept to determine accurately the SOH through the study of the loss of capacity during the ageing, more useful in applications where the batteries are subjected to a variable load. In the ToE a BF (Belief Function) is evaluated to define the degree of confidence that a particular event occurs. If $H$ is a general hypothesis, the BF can be evaluated as:

$$Bel(H) = \sum_{A_i \subseteq H} m(A_i) \tag{7}$$

where $m(A_i)$ are the masses that represent the empirical evidence which supports the $A_i$ possibility. A set of masses is defined as a body of evidence $\{m(A_1), m(A_2),\ldots, m(A_i), m(\Theta)\}$. The follows relation is verified:

$$\sum_{i=1}^{N} m(A_i) + m(\Theta) = 1 \tag{8}$$

where $m(\Theta)$, defined 0 in the classic Theory of Probability, indicates how insufficient is the evidence in support of the event $A$. The BF is

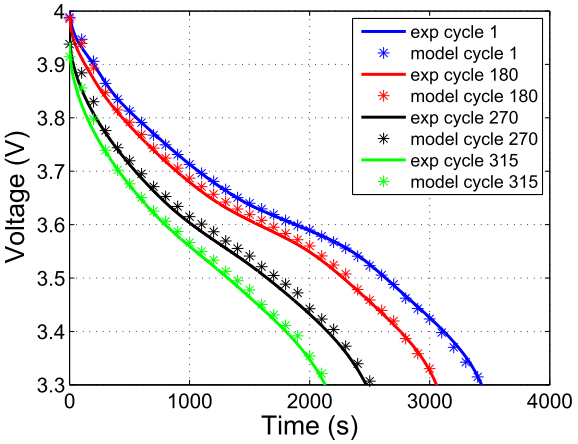


**Fig. 11.** Reproduction of the discharge curves of the battery through the equivalent circuit model of the battery. A comparison between model and experimental results.

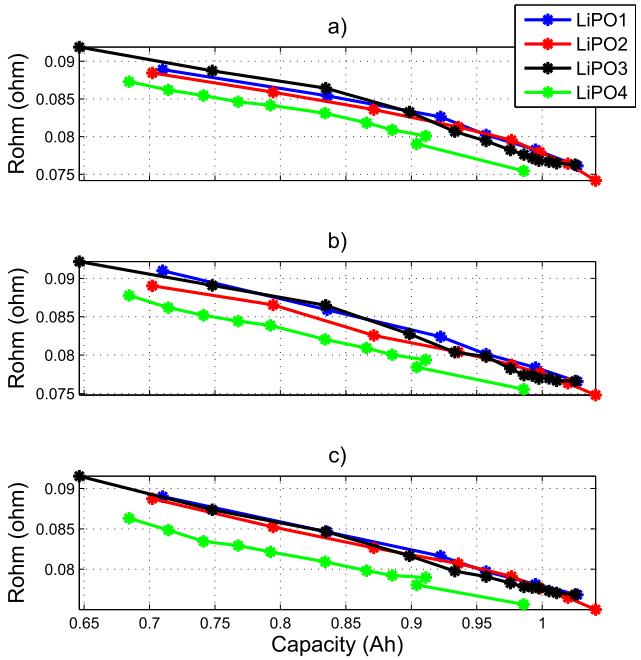


**Fig. 12.** Diagnostic relation between the ohmic resistance and the available capacity of the battery. a) Points acquired at SOC = 100%. b) SOC = 70%. c) SOC = 40%.

therefore defined as the sum of all the empirical evidence contained in hypothesis $H$. The Dempster-Schafer rule permits to combine the masses, putting in evidence compatible elements and neglecting contradicting ones. If $A_i$ and $B_j$ are two subsets of the frame of discernment, we can define two bodies of evidence $m(A_i)$ and $m(B_j)$, then for Dempster-Schafer rule, the combined body of evidence $m(C_Z)$ can be defined:

$$m(C_z) = \frac{\sum_{A_i \cap B_j = C_z} m(A_i)m(B_j)}{1 - \sum_{A_i \cap B_j = \varnothing} m(A_i)m(B_j)} \tag{9}$$

The numerator of the expression is the influence of the second empirical evidence aspects that confirm the first. The denominator is the complement to one of the second empirical evidence aspects that contradict the first. To determine the SOH, we use the map already introduced in Fig. 7. In this case the axes are reversed ($R_{ohm}$ on the x axis and SOC on the y axis, both with normalized values) and it is shown in Fig. 13. The curves of the reference battery, that we have assigned to the cell number 2 of Fig. 12, are reported in black. As previously introduced, we have acquired the data at different number of cycles every 45 charges and discharges, so we have built the curves of the map with a linear interpolation between the experimental ones. The coloured curves belong to the tested cells. The following analysis takes into considerations 9 cases: the tested LiPO 1 at cycles 1, 90 and 135, the tested LiPO 3 at cycles 1, 360 and 450, the tested LiPO 4 at cycles 1, 180 and 405. The masses assume the following form:

$$m(A_i) = k_m e^{-d_i} \tag{10}$$

where $d$ is the minimum distance of the trial points from the 315 cycles of the reference cell, while parameters $k$ represent the weight of the masses and can be calculated from the relation:

$$\sum_{i=1}^{N} k_m e^{-d_i} + m(\Theta) = 1 \tag{11}$$

We have chosen the uncertainty mass $m(\Theta)$ like a constant value of 0.1, and can be related to possibilities unknown, for example an error during the experimental test, due to a different battery temperature, or an error in the cell connections. The higher the mass values the more the measured cycle can be considered close to a specific reference one. We use the concept of the ToE in the following way: through a coulomb counting or a KF method (robust when the initial SOC is not known [48]), we determine the SOC and we acquire the ohmic resistance of the tested cell from the IS. We place the point on the diagnostic map and we determine the relative mass through eq. (10). When only one point is considered, the BF is simply the mass $m(A_i)$, where i is the number of cycles. After a small discharge of the battery, it is possible to acquire the new point and assign a mass $m(B_i)$. Then we combine the masses $m(A_i)$ and $m(B_i)$ through eq. (9) to determine a third mass $m(C_i)$, putting in evidence the compatible elements between the two masses and neglecting contradicting ones. The mass $m(C_i)$ can then replace the $m(A_i)$ in Eq. (9) in the next iterative cycle. The new $m(B_i)$ is then the third point at different SOC of the tested battery. The new $m(C_i)$ contains the combined information of the three points at different SOC of the tested battery. The iterative process can be repeated in an undefined way until points at different SOC are available and the battery is not completely discharged. When more points ($R_{ohm}(SOC)$) are available, the BF is the resulting mass $m(C_i)$. For the assumptions of the ToE, the points can be combined in a different order without changes in the results. Finally, the algorithm assigns an equivalent cycle from which we can determine the error in the evaluation of the SOH. The error can be extracted from the following equation:

$$err = \frac{C_{ref} - C_{test}}{C_{ref}} \tag{12}$$

where $C_{ref}$ is the capacity of the cell in Ah of the equivalent cycle obtained from the ToE, while $C_{test}$ is the capacity value relative to the cycle test. So from these assumptions it is not important if the batteries have a different cycle life, because the SOH is obtained from the capacity of the relative cycle of the cells. As first example, we consider the tested LiPO 1 at cycle 1. The result of the ToE is shown in Fig. 14, that reports the BF versus the number of cycles. In the figure, *Bel*1 represents the BF when only the first point at SOC 100% of the tested LiPO 1 is considered. The peak in the figure is the equivalent cycle that the ToE extracts from the diagnostic map. When the second point at different SOC is acquired, the BF is obtained combining the masses associated to the points through the Dempster-Schafer rule. We obtain *Bel*2. When all the points at different SOC are considered, the result of the ToE is *Bel*11. From Fig. 14, the peak of the BF with the number of points at different SOC reduces. This behaviour depends from the trend of the ohmic resistance versus SOC, as shown in the map of Fig. 13. Indeed, at low SOC, the ohmic resistance shows bigger variations than high SOC,

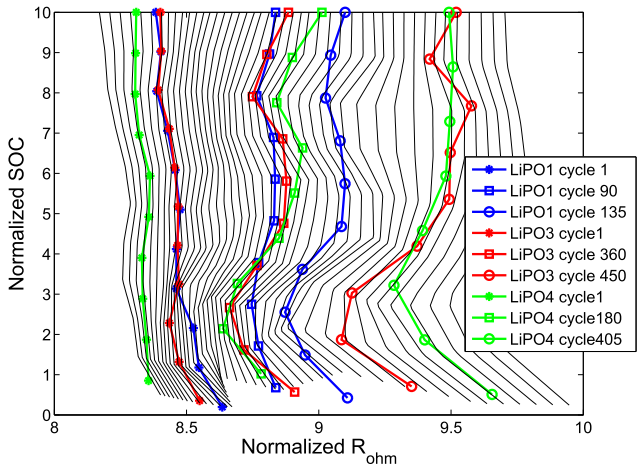


**Fig. 13.** Diagnostic map. The curves of the reference battery are reported in black. The tested batteries are reported in coloured lines.

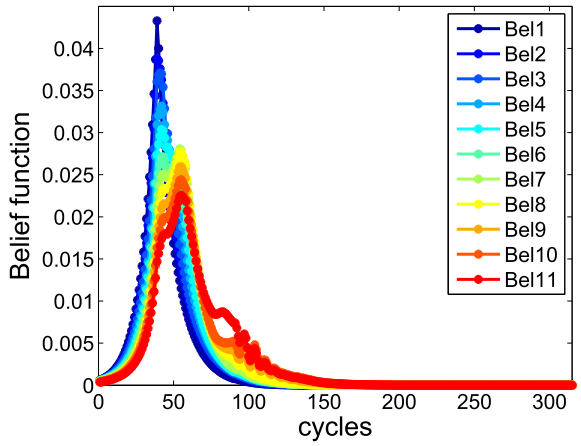


**Fig. 14.** Belief function of the tested LiPO 1 at cycle 1. *Bel*1, *Bel*2,…, *Beli* represent the new estimation of the BF as the points at different SOC are available and are combined through the Dempster-Schafer rule.

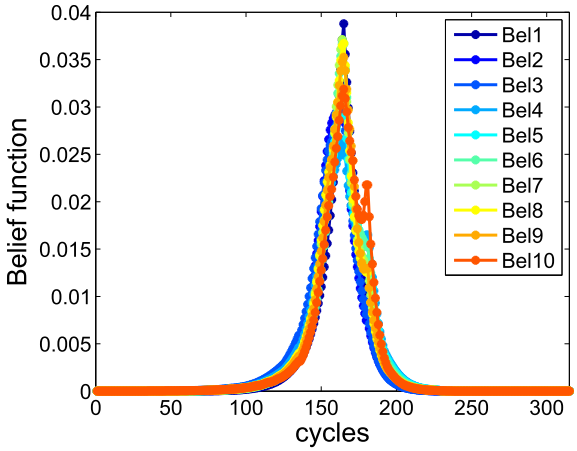


**Fig. 15.** Belief function of the tested LiPO 3 at cycle 360. *Bel*1, *Bel*2,…, *Beli* represent the new estimation of the BF as the points at different SOC are available and are combined through the Dempster-Schafer rule.

so the estimation of the ToE worse. From this consideration, it is evident that this method works also when only one point is acquired and placed in the map, avoiding the complete discharge of the battery. In this paper however we report the error in the evaluation of the SOH when all the points at different SOC are acquired, because this represents the worst case. In the case of Fig. 14, the evaluated error between the released capacity associated to the cycle extracted by ToE (cycle obtained observing the peak of *Bel*11) and the tested cycle is 1.18%. The results of the ToE when the tested LiPO 1 has been cycled 90 and 135 times show an error of respectively 0.25% and 3.3% in the evaluation of the SOH. To further validate the method, we have used the same procedure to determine the SOH of the tested LiPO 3 of Fig. 12. A representative result of the ToE is reported in Fig. 15, that shows the equivalent cycle extracted by the ToE when the tested LiPO 3 has been cycled 360 times. The error extracted by the ToE is limited and it is equal to 0.83%, 1.72% and 3.73% respectively for the tested battery cycled 1, 360 and 450 times. As it is possible to see from the results, the error in the evaluation of the SOH increases at low SOH. This is due to a bigger loss of capacity when the SOH enhances, causing an increment of the error in the SOH evaluation. Nevertheless the error is limited, with a maximum value of 3.73%. Finally we report the results obtained on the tested LiPO 4, cycled 1, 180 and 405 times. A representative result of the ToE is reported in Fig. 16 (cell cycled 405 times). The error in the evaluation of the SOH when the battery is cycled 1, 180 and 405 times is respectively 4.22%, 7.95% and 8.66%. The errors for LiPO 4 are higher, however, in Fig. 12 it is possible to notice that the cell has an anomalous behaviour. Indeed, it has released during the ageing a smaller value of capacity compared to the other cells and it has shown a drastic loss of capacity during the initial 45 cycles, following a light recovery between 45th and 90th cycles. The small value of error obtained by the ToE verifies the robustness of the method, also when batteries with anomalous behaviours are considered. Summarizing, when only standard cells are considered, the maximum error of the ToE in the evaluation of the SOH is 3.73%, with a peak of 8.66% when the anomalous cell is considered.

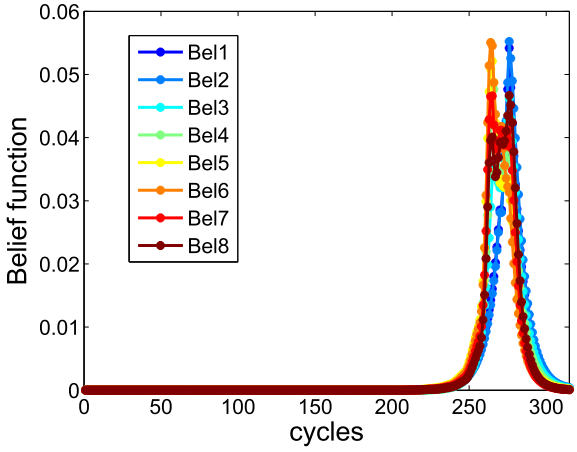


**Fig. 16.** Belief function of the tested LiPO 4 at cycle 405. *Bel*1, *Bel*2,…, *Beli* represent the new estimation of the BF as the points at different SOC are available and are combined through the Dempster-Schafer rule.

## 5. Conclusion

In this paper, we have performed a characterization of lithium polymer batteries through EIS to study the performance under load and the SOH through the ToE. Compared to other methods, EIS is a powerful diagnostic tool to study the physical and chemical properties of any electrochemical system, allowing the possibility to study physical parameters for the monitoring of the batteries. We have extracted the parameters of an equivalent circuit model through a fitting procedure of the IS at different SOC and SOH, and in the following we have used these parameters to reproduce the discharge curves of the batteries, useful in the applications where the power behaviour of the battery is important, to study the voltage performance and possibly evaluate the SOC. The discharge curves are however not useful to evaluate the SOH, since the batteries cannot be discharged completely when they are integrated in hybrid energy production systems. For this reason we have built a diagnostic map, that shows the variation of the ohmic resistance of the battery with the SOC. We have interpreted the diagnostic map through the ToE. The method is versatile and adaptable when more diagnostic maps are identified (through the Dempster-Schafer rule it is possible to improve the estimation of the SOH). The maximum error in the evaluation of the SOH is 3.73% when standard cells are considered, with an enhancement to 8.66% when an anomalous battery is considered. The method is therefore solid to real conditions, where there is the possibility to meet batteries with different behaviours, also when these cells belong to the same technology, with the same voltage and nominal capacity. In the future this work could be integrated with already existing techniques based on the battery model, for example the KF theory, in order to improve not only the model itself but also the estimation goodness of the key parameters (e.g. SOC). Moreover, it will be implemented a parallel acquisition of all the harmonic signals (multisine approach) [49] in order to work under realistic operative conditions where the load is variable in time.

## Acknowledgements

We gratefully acknowledge support from Telecom Italia. Special thanks to Alena Trifirò and Ilaria Perissi for useful discussions.

## References

[1] Scrosati B, Garche J. Lithium batteries: status, prospects and future. J Power Sources 2010;195:2419–30.
[2] Takami N, Inakagi H, Tatebayashi Y, Saruwatari H, Honda K, Egusa S. High-power and long-life lithium-ion batteries using lithium titanium oxide anode for automotive and stationary power applications. J Power Sources 2013;244:469–75.
[3] Wu H, Cui Y. Designing nanostructured Si anodes for high energy lithium ion batteries. Nano Today 2012;7:414–29.

[4] Dali M, Belhadj J, Roboam X. Hybrid solar-wind system with battery storage operating in grid-connected and standalone mode: control and energy management - experimental investigation. Energy 2010;35:2587–95.
[5] Sanseverino ER, Di Silvestre ML, Ippolito MG, De Paola A, Lo Re G. An execution, monitoring and replanning approach for optimal energy management in microgrids. Energy 2011;36:3429–36.
[6] Lu L, Han X, Li J, Hua J, Ouyang M. A review on the key issues for lithium-ion battery management in electric vehicles. J Power Sources 2013;226:272–88.
[7] Waag W, Fleischer C, Sauer DU. Critical review of the methods for monitoring of lithium-ion batteries in electric and hybrid vehicles. J Power Sources 2014;258:321–39.
[8] Barrè A, Deguilhem B, Grolleau S, Gérard M, Suard F, Riu D. A review on lithium-ion battery ageing mechanisms and estimations for automotive applications. J Power Sources 2013;241:680–9.
[9] Hu X, Li SE, Jia Z, Egardt B. Enhanced sample entropy-based health management of Li-ion battery for electrified vehicles. Energy 2014;64:953–60.
[10] Broussley M, Biensan P, Bonhomme F, Blanchard P, Herreyre S, Nechev K, et al. Main aging mechanisms in Li ion batteries. J Power Sources 2005;146:90–6.
[11] Peterson SB, Apt J, Whitacre JF. Lithium-ion battery cell degradation resulting from realistic vehicle and vehicle-to-grid utilization. J Power Sources 2010;195:2385–92.
[12] Nagpure SC. Multi-scale characterization studies of aged Li-ion battery materials for improved performance [Phd thesis]. The Ohio State Univ.; 2012.
[13] Schalkwijk W, Scrosati B. Advances in lithium-ion batteries. New York: Kluwer Accademic Publishers; 2002. p. 393–432.
[14] Fang W. Ageing fundamental modeling the performance and degradation of HEV Li-ion battery [Phd thesis]. Pennsylvania State Univ.; 2010.
[15] Wright RB, Christophersen JP, Motloch CG, Belt JR, Ho CD, Battaglia VS, et al. Power fade and capacity fade resulting from cycle-life testing of advanced technology development program lithium-ion batteries. J Power Sources 2003;119–121:865–9.
[16] Plett GL. Extended Kalman filtering for battery management systems of LiPB-based HEV battery packs. Part 3. State and parameter estimation. J Power Sources 2004;134:277–92.
[17] Sun F, Hu X, Zou Y, Li S. Adaptive unscented Kalman filtering for state of charge estimation of a lithium-ion battery for electric vehicles. Energy 2011;36:3531–40.
[18] Haifeng D, Xuezhe W, Zechang S. A new SOH prediction concept for the power lithium-ion battery used on HEVs. In: Vehicle Power and Propulsion Conference VPPC'09, Dearborn, 7-10 Sept; 2009. p. 1649–53.
[19] Xiao-song H, Feng-chun F, Yuan Z. Online model identification of lithium-ion battery for electric vehicles. J Cent South Univ Technol 2011;18:1525–31.
[20] Hu Y, Yurkovich S, Guezennec Y, Yurkovich BJ. A technique for dynamic battery model identification in automotive applications using linear parameter varying structures. Control Eng Pract 2009;17:1190–201.
[21] Huet F. A review of impedance measurements for determination of the state-of-charge or state-of-health of secondary batteries. J Power Sources 1998;70:59–69.
[22] Canas NA, Hirose K, Pascucci B, Wagner N, Friedrich KA, Hiesgen R. Investigations of lithium-sulfur batteries using electrochemical impedance spectroscopy. Electrochim Acta 2013;97:42–51.
[23] Popp H, Einhorne M, Conte FV. Capacity decrease vs. Impedance increase of lithium batteries. A comparative study. In: Hybrid and Fuel Cell Electric Vehicle Symposium & Exhibition EVS26, Los Angeles; 6-9 May, 2012.
[24] Eddahech A, Briat O, Vinassa JM. Performance comparison of four lithium-ion battery technologies under calendar aging. Energy 2015. http://dx.doi.org/10.1016/j.energy.2015.03.019.
[25] Seki S, Kobayashi Y, Miyashiro H, Yamanaka A, Mita Y, Iwahori T. Degradation mechanism analysis of all-solid-state lithium polymer secondary batteries by using the impedance measurement. J Power Sources 2005;146:741–4.
[26] Troltzsch U, Kanoun O, Trankler H. Characterizing aging effects of lithium ion batteries by impedance spectroscopy. Electrochim Acta 2006;51:1664–72.
[27] Eddahech A, Briat O, Henry H, Deletage JY, Woirgard E, Vinassa JM. Ageing monitoring of lithium-ion cell during power cycling tests. Microelectron Reliab 2011;51:1968–71.
[28] Eddahech A, Briat O, Bertrand N, Deletage JY, Vinassa JM. Behaviour and state-of-health monitoring of Li-ion batteries using impedance spectroscopy and recurrent neural networks. Electr Power Energy Syst 2012;42:487–94.
[29] Waag W, Kabitz S, Sauer DU. Experimental investigation of the lithium-ion battery impedance characteristic at various conditions and aging states and its influence on the application. Appl Energy 2013;102:885–97.
[30] Shim J, Kosteki R, Richardson T, Song X, Striebel KA. Electrochemical analysis for cycle performance and capacity fading of a lithium-ion battery cycled at elevated temperature. J Power Sources 2002;112:222–30.
[31] Ning G, Haran B, Popov BN. Capacity fade study of lithium-ion batteries cycled at high discharge rates. J Power Sources 2003;117:160–9.
[32] Spotniz R. Simulation of capacity fade in lithium-ion batteries. J Power Sources 2003;113:72–80.
[33] Gould CR, Bingham CM. New battery model and state-of-health determination through subspace parameter estimation and state-observer techniques. IEEE Trans Veh Technol 2009;58:3905–16.
[34] Barsoukov E, Macdonald R. Impedance spectroscopy, theory, experiment, and applications. Hoboken: John Wiley & Sons Inc.; 2005. p. 461–2.
[35] Vetter J, Novak P, Wagner MR, Veit C, Moller KC, Besenhard JO, et al. Ageing mechanisms in lithium-ion batteries. J Power Sources 2005;147:269–81.
[36] Schweighofer B, Raab KM, Brasseur G. Modeling of high power automotive batteries by the use of an automated test system. IEEE Trans Instrum Meas 2003;52:1087–91.
[37] Pop V, Bergveld HJ, Notten PHL, Regtien PPL. State-of-the-art of battery state-of-charge determination. Meas Sci Technol 2005;16:R93–110.
[38] Lee Y, Cheng M. Intelligent control battery equalization for series connected lithium-ion battery strings. IEEE Trans Ind Electron 2005;52:1297–307.
[39] Xu L, Ruan X, Mao C, Zhang B, Luo Y. An improved optimal sizing method for wind-solar-battery hybrid power system. IEEE Trans Sustain Energy 2013;4:774–85.
[40] Xiong R, He H, Sun F, Liu X, Liu Z. Model-based state of charge and peak power capability joint estimation of lithium-ion battery in plug-in hybrid electric vehicles. J Power Sources 2013;229:159–69.
[41] Bruni G, Cordiner S, Galeotti M, Mulone V, Nobile M, Rocco V. Control strategy influence on the efficiency of a hybrid photovoltaic-battery-fuel cell system distributed generation system for domestic applications. Energy Procedia 2014;45:237–46.
[42] Krieger EM, Cannarella J, Arnold CB. A comparison of lead-acid and lithium-based battery behaviour and capacity fade in off-grid renewable charging applications. Energy 2013;60:492–500.
[43] Wolfahrt-Meherens M, Vogler C, Garche J. Aging mechanisms of lithium cathode materials. J Power Sources 2004;127:58–64.
[44] Dubarry M, Liaw BY. Identify capacity fading mechanism in a commercial LiFePO4 cell. J Power Sources 2009;194:541–9.
[45] Broussely M, Herreyre S, Biensan P, Kasztejna P, Nechev K, Staniewicz RJ. Aging mechanism in Li ion cells and calendar life predictions. J Power Sources 2011;97–98:13–21.
[46] Salicone S. Measure uncertainty: an approach via the mathematical theory of evidence. Springer Science+Business Media LLC; 2007. p. 31–67.
[47] Galeotti M, Giammanco C, Cinà L, Cordiner S, Di Carlo A. Synthetic methods for the evaluation of the state of health (SOH) of nickel-metal hydride batteries. Energy Convers Manag 2015;92:1–9.
[48] Spagnol P, Rossi S, Savaresi SM. Kalman filter SoC estimation for Li-ion batteries. In: IEEE International Conference on Control Applications (CCA), Denver, sept. 28-30; 2011. p. 587–92.
[49] Sanchez B, Louarroudi E, Jorge E, Cinca J, Bragos R, Pintelon R. A new measuring and identification approach for time-varying bioimpedance using multisine electrical impedance spectroscopy. Physiol Meas 2013;34:339–57.